Thin Solid Films, 200 (1991) 49–66

THE QUENCHING STRESS IN THERMALLY SPRAYED COATINGS

S. KURODA* AND T. W. CLYNE
Department of Materials Science and Metallurgy, Pembroke Street, Cambridge CB2 3QZ (U.K.)
(Received August 17, 1990; accepted November 19, 1990)

Various material properties which influence residual stresses in plasma-sprayed deposits are examined. A simple expression to evaluate the residual stress in a plasma-sprayed coating is given for the case where the coating thickness is much smaller than the substrate thickness. The equation contains two terms, the stress owing to quenching of sprayed splats and the macroscopic thermal stress arising from differential thermal contraction. The variables in the equation have been studied experimentally.

Methods of measuring the quenching stress are described and values are reported for a wide range of materials and deposition conditions. For metallic powders, correlation can be established between the magnitude of the quenching stress and the propensity of the material to undergo creep deformation and/or plastic yielding. For a ceramic powder such as Al_2O_3 this is not possible and the quenching stress is very low. Mechanisms are suggested for the reduction in the quenching stress, microcracking being a prominent suggestion. Poor bonding between splats and the incorporation of small disintegrated particles are probably also of significance.

Mechanical and thermal properties of sprayed materials, such as Young's modulus and the coefficient of thermal expansion, have been measured. Effects of porosity are examined using the Eshelby equivalent homogeneous inclusion method. The importance of using measured *in situ* properties in quantitative modelling work is emphasized.

1. INTRODUCTION

Residual stress in plasma-sprayed coatings has been recognized as one of their most important characteristics. It can give rise to deformation of coated workpieces and spallation or cracking of the coating. In addition, various types of coating performance indicators, such as adhesion strength[1,2], resistance to thermal shock,

* On leave from: Advanced Materials Processing Division, National Research Institute for Metals, 2-3-12 Nakameguro, Meguro-ku, Tokyo 153, Japan.

0040-6090/91/$3.50

life under thermal cycling[3] and erosion resistance[4], are strongly influenced by the nature of the residual stresses.

It seems clear that the following sources of stress generation operate during the spraying process.

1. Stress owing to contraction of individual sprayed splats as they rapidly cool to the substrate temperature. This is the "quenching stress". It is always tensile in the splats.
2. Differential thermal contraction stress. This arises as the substrate and deposit cool together, with or without thermal gradients. It is macroscopic because the bulk of sprayed deposit can be considered as a continuous solid. Depending on the thermal expansivities and the thermal gradient, it can be either tensile or compressive in the deposit.
3. Volume change associated with any solid state phase transformations[5,6].

Of these stresses, the stress resulting from contraction of individual splats is specific to the spraying process and is probably the most difficult to calculate theoretically. The origin of the stress is constraint by the underlying solid body on the thermal contraction of sprayed splats, as shown schematically in Fig. 1. As a molten particle strikes the surface of a solid it spreads out and forms a flat splat, rapidly losing heat through conduction to the underlying solid. It is known that the solidification and subsequent cooling of a single particle can be treated as independent events under normal spraying conditions[7]. As the particle cools down its thermal contraction is somewhat constrained, the degree of constraint depending on the nature of the bonding at the interface and the geometry of the splat.

Table I shows handbook values at room temperature of thermal expansivity, Young's modulus, thermal strain arising from a temperature drop of 100 K and the

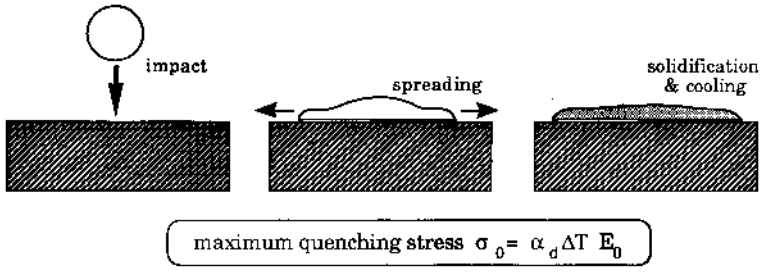

Fig. 1. Schematic depiction of impact, spreading and cooling of a single splat.

TABLE I
COMPARISON OF STRAIN AND STRESS FROM THERMAL CONTRACTION FOR A RANGE OF MATERIALS

Material	α_0 (10^{-6} K^{-1})	E_0 (GPa)	$\alpha_0 \Delta T$ (mstrain for ΔT = 100 K)	$\alpha_0 \Delta T E_0$ (MPa)
Molybdenum	4.9	325	0.49	160
Nickel	12.8	200	1.28	255
Aluminium	23	71	2.3	162
Al_2O_3	8	370	0.8	300

corresponding stress if the strain were completely constrained. It indicates that even for this relatively small ΔT of 100 K, stresses higher than 100 MPa can readily develop. Supposing that the interfacial bonding between the splat and the underlying solid is perfect and the temperature change experienced by the splat during cooling is sufficiently large, then lateral tensile stress which is much higher than the yield strength under uniaxial loading can readily develop. This is because plastic flow in a thin film strongly bonded to a rigid substrate is strongly constrained. However, there are a number of stress relaxation processes which may operate to reduce the stress in the splat below its maximum value σ_0 (Fig. 2). The key question concerns the degree to which these stress relaxation processes can in practice reduce the quenching stress below its theoretical value. For example, if the material is brittle, microcracking can reduce the stress significantly.

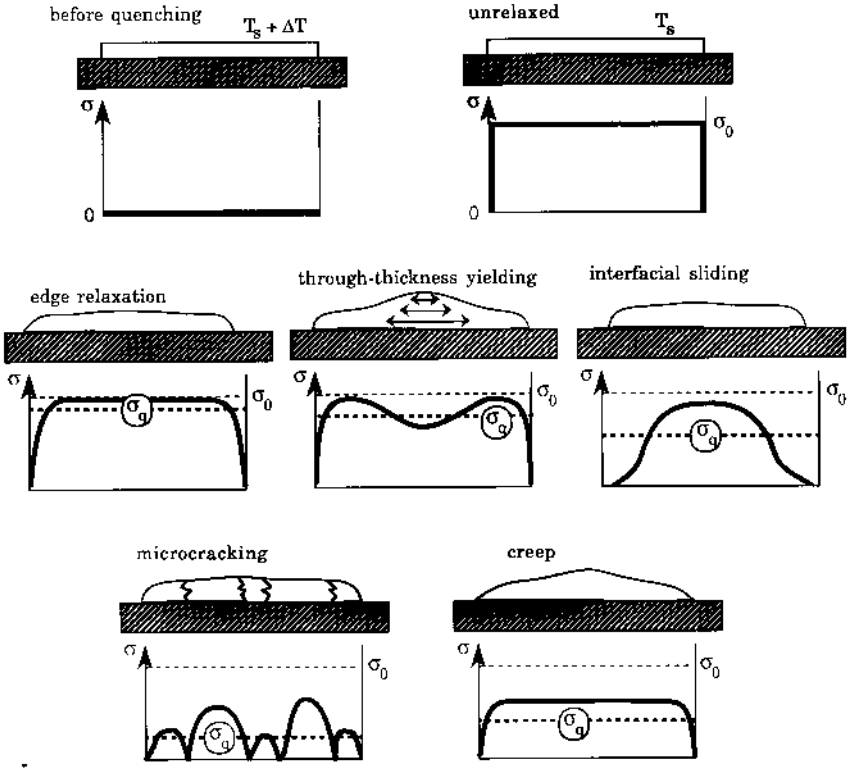

Fig. 2. Schematic illustration of the stress distributions within a single splat before and after various stress relaxation phenomena have taken place.

Even though the existence of the quenching stress has been suggested[8,9], no quantitative data have been reported until recently[10] and most workers have only considered macroscopic thermal stress arising from thermal gradients or mismatch in thermal expansivity between the coating and the substrate[4,11,12].

Recently much effort has been put into the development of numerical models to predict the stress distribution in the plasma-sprayed coatings in order to understand

thermal and mechanical phenomena during spray deposition and to optimize the stress state for specific applications,[12,13–16]. By comparing model predictions with observed curvature changes Gill and Clyne pointed out that: the stress due to quenching needs to be properly incorporated into a model; and materials properties must be properly evaluated in order to predict the stress state of sprayed deposits correctly[14–16].

Even though it has been long recognized that some thermal and mechanical properties of sprayed deposits are markedly different from dense bulk materials, there seem to be few systematic data or analyses available.

2. A SIMPLE MODEL FOR RESIDUAL STRESS GENERATION

The significance of this quenching stress on the final state of residual stress can best be understood by considering a simple model in which

1. the coating thickness h_d is negligible compared with the thickness h_s of the substrate,
2. spraying is done onto a substrate held at a constant temperature T_s,
3. the sprayed deposit is quenched to T_s instantaneously, and
4. the substrate–deposit couple remains isothermal as it cools down to the ambient temperature T_0.

This is similar to practical spraying conditions with preheating and adequate cooling during spraying. By further supposing that the interfacial bonding between the deposit and the substrate is perfect and the materials behave elastically in the cooling period, then the final residual stress $\sigma_r(T_0)$ in the deposit can be expressed simply as the sum of the quenching stress and that arises from differential thermal contraction

$$\sigma_r(T_0) = \{\sigma_q(T_s)/E_d(T_s) + (\alpha_d - \alpha_s)(T_s - T_0)\}E_d(T_0) \quad (1)$$

where $\sigma_q(T_s)$ is the average of the lateral stress built up in the splats as shown in Fig. 2, $E_d(T)$ is the value of the Young's modulus of the coating at temperature T and α_d and α_s are the thermal expansivities of the deposit and the substrate respectively. Figure 3 shows the dependence of the residual stress σ_r on the substrate temperature

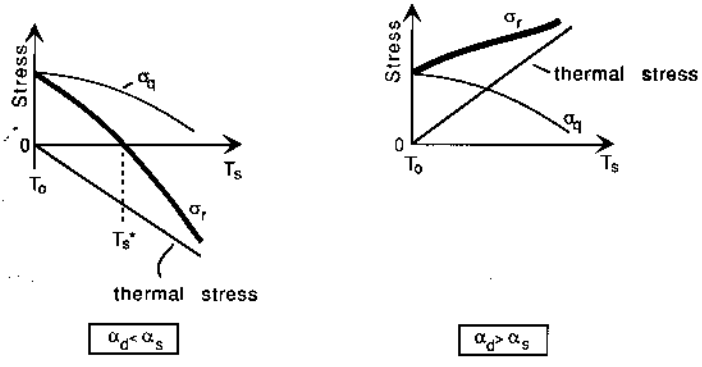

Fig. 3. Schematic diagram of the variation of the final residual stress with substrate temperature T_s during spraying. $\sigma_r(T_0)$ is the final residual stress after the sprayed deposit and the substrate cool down to T_0.

T_s. Obviously if $\alpha_d = \alpha_s$ or $T_s = T_0$ no thermal stress is generated and the quenched strain in the sprayed deposit is preserved. For $\alpha_d < \alpha_s$ the stress in the deposit becomes more compressive as T_s is raised: the sign of the net residual stress changes from tensile to compressive at $T_s = T_{s*}$ given by the relation

$$T_{s*} = \frac{\sigma_q(T_{s*})}{E_d(T_{s*})(\alpha_s - \alpha_d)} + T_0 \tag{2}$$

and the final stress is compressive for T_s values higher than this. For $\alpha_d > \alpha_s$, there is no reversal in the sign of residual stress, which is always tensile and increases with T_s. This simple scheme agrees well with experimental observations in a previous work[17]. The main uncertainty concerns the influence of stress relaxation phenomena on the σ_q curve. (These processes will also affect the differential thermal contraction stress, but the change is likely to be less significant because of the lower temperature and the absence of free surfaces.)

Recently one of the authors of this paper developed a technique to measure the quenching stress by continuously monitoring the curvature change of a substrate during spraying. It was shown that the stress becomes independent of substrate material when the coating thickness exceeds about 10 μm[10,17]. The stress, measured by depositing four kinds of metallic powder (molybdenum, nickel, aluminium and 80Ni–20Cr alloy), was always tensile; ranging from 10 to 100 MPa in the order of Al ≈ Mo < Ni < 80Ni–20Cr alloy. (The term "quenching stress" is used in this paper instead of "deposition stress" in the previous papers[10,17] because "quenched" describes the nature of the stress more clearly.)

In the present paper, the dependence of the quenching stress on substrate temperature and the spraying environment is studied systematically. Vacuum plasma spraying (VPS) is employed to explore the stress behaviour at higher temperature, whereas conventional spraying in air (APS) is employed to cover a lower temperature range attainable by efficient air cooling. Mechanical and thermal properties such as Young's modulus and coefficient of thermal expansion are measured and compared with some model calculations where possible. The implications of thermal and mechanical properties in interpreting the measured stress and final residual stress are discussed.

3. EXPERIMENTAL PROCEDURE

3.1. Powder characteristics and spraying conditions

Purity and size of spray powders are listed in Table II. Spraying conditions for both APS and VPS are shown in Table III.

3.2. Measurement of Young's modulus

Three-point bending was employed to measure the Young's modulus of deposits sprayed with APS. To see the effects of substrate temperature during spraying, each powder was sprayed onto a strip-shaped substrate, with maximum cooling provided by an air blast and also without cooling for comparison. When cooling was performed, the temperature of the substrate could be kept below 100 °C, whereas when there was no cooling it was between 400 and 500 °C. Since the coating

TABLE II
LIST OF POWDER CHARACTERISTICS

Material	*Purity or composition* (wt%)	*Size* (μm)
Aluminium	99.76	−88 + 10
Nickel	99	−44 + 10
Molybdenum	99.8	−53 + 10
80Ni–20Cr	Ni = 79.2, Cr = 19.7	−44 + 10
Al_2O_3	99.8	−44 + 10

should ideally be removed from the substrate for the measurement, a very thin layer of tin was sprayed onto the substrate first, then a coating of thickness 1–2 mm was sprayed. This was subsequently removed by heating to melt the tin layer. After gently grinding off the tin layer with abrasive paper, the thickness of the deposit was measured with a micrometer.

The above technique is not applicable to the case where the substrate is at high temperature. For some materials with poor adhesion to the substrate (such as Al_2O_3) or with large quenching stress (such as 80Ni–20Cr) the coatings tend to peel off spontaneously during spraying and could be easily removed after spraying. However, for materials such as molybdenum and aluminium, it is difficult to remove a coating from the substrate and therefore the modulus of the coating was calculated by measuring the flexural rigidity of the composite beam[18], using handbook data for the substrate (which is taken to be fully dense).

3.3. *Measurement of thermal expansivities*

The coefficient of thermal expansion was measured by using an interferometric dilatometer[19], in which specimens are inserted between a pair of glass plates forming a cavity in a Fizzeau interferometer, as shown in Fig. 4. The dilation of the specimen is measured by counting the number of interference fringes using a photo-detector and hence resolution better than $\lambda/4$ (λ = 632.8 nm: the wavelength of helium–neon laser used) is easily attained. Specimens were cut from those used for modulus measurement and the dilation in the through-thickness direction was measured in air from room temperature to about 300 °C.

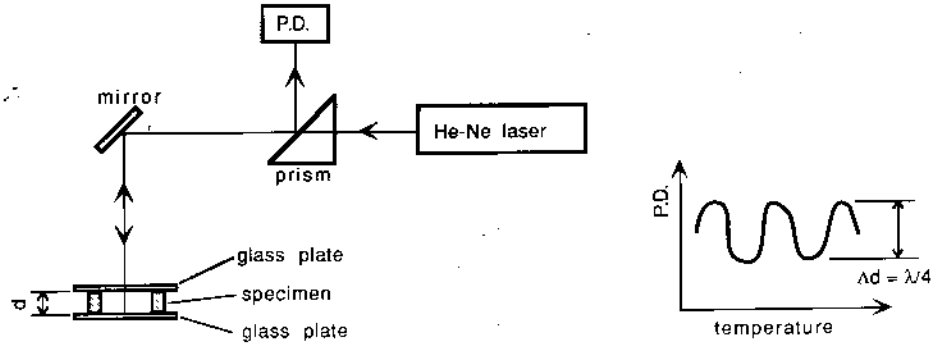

Fig. 4. Schematic diagram of the laser interferometric dilatometer.

TABLE III

SPRAY CONDITIONS FOR VPS

Powder	*Plasma gas*		*Other parameters*				
	Primary, flow rate (1 min $^{-1}$)	*Secondary, flow rate* (1 min $^{-1}$)	*Arc current* (A) *voltage* (V)	*Feed rate* (g min $^{-1}$)	*Feed gas (Ar) flow rate* (1 min $^{-1}$)	*Chamber pressure* (mbar)	*Nozzle diameter* (mm)
Nickel	Ar, 50	H_2, 4	700A, 50V	38	2.5	200	7
80Ni–20Cr	Ar, 50	H_2, 4	700A, 50V	26	2.5	200	7
Molybdenum	Ar, 50	H_2, 10	700A, 60V	24	2	200	7

Spray distance, 300 mm; torch linear velocity, 0.1 m s $^{-1}$.

SPRAY CONDITIONS FOR APS

Powder	*Plasma gas, flow rate* (1 min $^{-1}$)	*Arc current* (A) *voltage* (V)	*Feed rate* (g min $^{-1}$)	*Feed gas flow rate* (1 min $^{-1}$)	*Nozzle diameter* (mm)
Aluminium	Ar, 45	600A, 30V	1	2.5	8
Nickel	Ar, 45	600A, 30V	8	2.5	8
80Ni 20Cr	Ar, 45	600A, 30V	10	2.5	8
Molybdenum	Ar, 45	600A, 30V	10	2	8
Al_2O_3	Ar, 45	600A, 30V	5	2.5	8

Spray distance, 100 mm; torch linear velocity, 0.18 m s $^{-1}$.

3.4. Measurement of the quenching stress

For spraying in air (APS), an *in situ* curvature measurement was employed to determine the stress by quenching[10,17]. The temperature of the substrate during spraying was controlled by the flow rate of air jets provided by a pair of nozzles attached to the plasma torch. Strip-shaped mild steel plates (2 mm × 15 mm × 100 mm) were blasted under conventional conditions with 500 μm alumina sand, annealed in a vacuum of 10^{-6} Torr (to remove residual stress from the blasting procedure) and then degreased in acetone before spraying. A substrate was then fixed on a pair of knife edges and the displacement at the centre on the rear face was measured continuously with a transducer during spraying, this displacement being proportional to the curvature ($1/R$) of the strip for small displacements. From the slope of the curvature change with respect to deposit thickness h_d, the average lateral stress $\sigma_q(T_s)$ developed in the deposit during quenching is given by the following equation (after Stoney[20])

$$\sigma_q(T_s) = \frac{E_s(T_s)h_s^2}{6} \frac{\delta}{\delta h_d}\left(\frac{1}{R}\right) \tag{3}$$

where $E_s(T_s)$ and h_s are the modulus of the substrate at temperature T_s and the thickness of the substrate respectively.

For spraying under reduced pressure (VPS), a slightly different approach was taken because of the unsuitability of the *in situ* instrument for the environment in the VPS chamber. As shown in previous work[17] for spraying of the same material as the substrate, the curvature at the end of spraying is retained because no thermal stress is generated during cooling. The thermal expansion coefficient should not vary with porosity content, stored stress etc. The validity of this was checked experimentally by video-recording the image of a specimen through a glass window[16]. Although the precision of curvature measurement is slightly less than that of the contacting method described above for APS, the technique gives good sensitivity for the detection of any changes during cooling to room temperature after spraying. Molybdenum and nickel substrates with similar dimensions and the same preparation procedure as that described above for mild steel were clamped to a specimen holder as shown in Fig. 5 and the temperature of the substrate was recorded by a

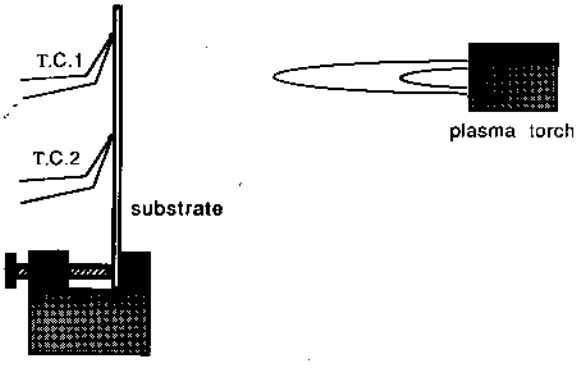

Fig. 5. Specimen set-up for vacuum plasma spray deposition.

pair of thermocouples spot-welded to the rear of the substrate. Coatings with thickness ranging from 0.1 to 0.4 mm were made by spraying molybdenum, nickel and 80Ni–20Cr powders and the temperature T_s of the substrate during spraying was defined as the average temperature measured by the two thermocouples throughout the spraying period. The portion of 70 mm length from the top, over which there was a fairly uniform temperature distribution, was used for curvature evaluation. This was done by measuring the surface profile of the rear face of each substrate by using a travelling microscope before and after spraying. The curvature $(1/R)$ was calculated from the profile change in order to eliminate error owing to initial deformation of the strip. Then the quenching stress $\sigma_q(T_s)$ was calculated by the following equation, given by Brenner and Senderoff[21]

$$\sigma_q(T_s) = \frac{E_s(T_s)h_s(h_s + \beta^{5/4}h_d)}{6\,R\,h_d} \tag{4}$$

where β is the modulus ratio $E_d(T_s)/E_s(T_s)$. The modulus $E_d(T_s)$ of the deposit at temperature T_s was taken as one third of the handbook value for the temperature concerned to take into account the effect of porosity, microcracking etc. and it is broadly consistent with a number of modulus measurements (see below). Obviously, for any specific case it would be preferable to use a value obtained for the coating concerned.

4. RESULTS AND DISCUSSION

4.1. Young's modulus data

Measured values of Young's modulus for sprayed materials E_d are compared with values for the corresponding dense materials E_0 in Fig. 6. The dashed line in the figure corresponds to $E_d = E_0/3$: data for the metallic deposits seem to lie around this line, whereas sprayed Al_2O_3 gives appreciably lower values. Judging from the results for nickel and molybdenum, the composite beam approach seems to give 20%–25% lower values than the values given by monolithic beams, which perhaps

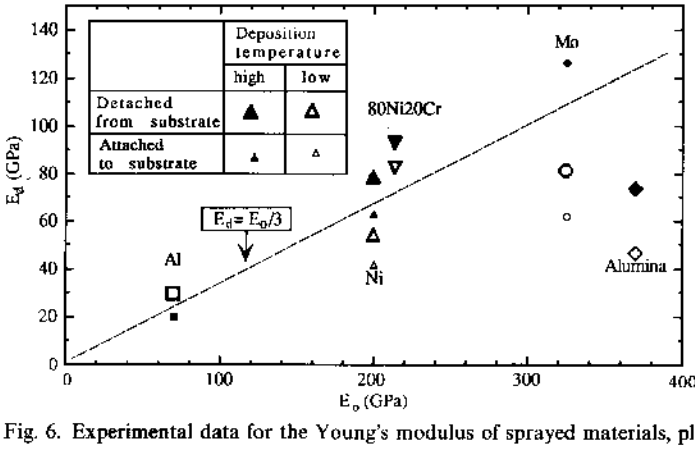

Fig. 6. Experimental data for the Young's modulus of sprayed materials, plotted as a function of the corresponding bulk (fully dense) values.

indicates that the assumption of perfect bonding between the coating and the substrate in the composite beam calculation may not be strictly valid and some sliding at the interface may occur during the measurement. Comparing the values for deposits sprayed at high and low temperatures, those at high temperatures have slightly higher moduli. This would be consistent with somewhat denser deposits being formed when the substrate temperature is higher.

The Eshelby equivalent homogeneous inclusion model[22], which treats porosity as randomly distributed ellipsoids with zero stiffness, has been applied to predict the modulus of APS deposits of Al_2O_3 and molybdenum, as shown in Fig. 7. The curves in the figure show the calculated modulus as a function of porosity volume fraction for three different values of pore aspect ratio S. As shown in Fig. 6, the measured modulus of the molybdenum was about one third of the bulk value while that of the Al_2O_3 ranged from 51 to 78 GPa (*cf.* handbook value of about 380 GPa). These experimental data are shown as blocks for a probable range of porosity from 5% to 10%. It was found that pores of a very high aspect ratio (approximately 1:100) resembling through-thickness cracks are necessary to reduce the modulus of γ-Al_2O_3 to the observed extent; even for molybdenum, an aspect ratio below 1:10 seemed appropriate. Since the model assumes the matrix to be a complete solid body, the possibility of poor bonding between splats could be partly responsible for these results.

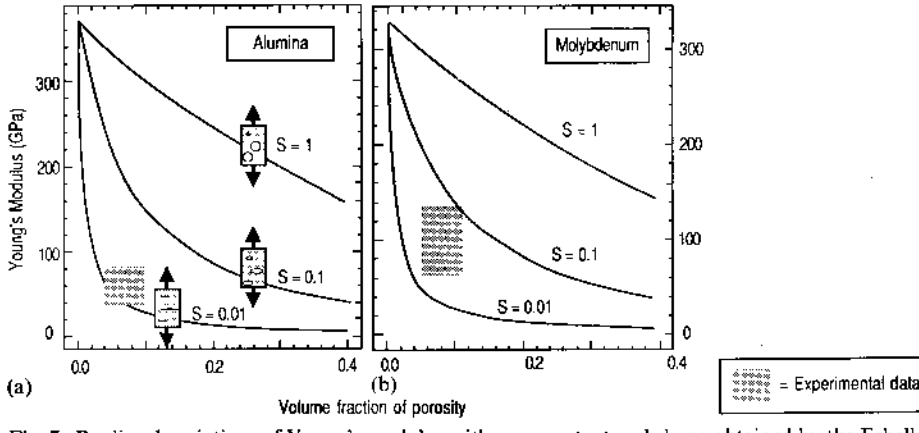

Fig. 7. Predicted variations of Young's modulus with pore content and shape obtained by the Eshelby method for (a) alumina and (b) molybdenum.

Direct observation of the bonding between Al_2O_3 splats was reported by McPherson and Shafer using transmission electron microscopy (TEM)[23]. They found that very thin gaps with thickness of 0.01–0.1 μm exist between splats and, hence, the real area of contact is rather small. Reported reduction in rigidity and Poisson's ratio[24] were attributed to the gaps suggested to result from entrapped gas between the impinging droplet and substrate.

Noutomi *et al.* measured residual stress in Ni–Cr alloy and ZrO_2–20%Y_2O_3 plasma-sprayed in air using both X-ray diffraction and stress relaxation after cutting. They found general agreement between these two methods[25]. They also

showed that the Young's moduli measured by three point bending are about 1/4–1/5 of the bulk values for the Ni–Cr alloy deposits and 1/18 of the ZrO_2–20%Y_2O_3. The ratio of the X-ray stress constant[26] $E/(1+\nu)$ determined experimentally to the value derived from bulk values of E and ν is only 1/1.3 to 1/2. It was suggested that a significant portion of strain is accommodated not within the solid splats but in the oxides or gaps between the splats. Therefore it cannot be detected by the X-ray method.

4.2. Thermal expansivity data

Measured coefficients of linear thermal expansion of various sprayed materials are plotted against standard bulk values in Fig. 8. Even though there seems to be a considerable scatter in the data, those values are in general agreement. Pores should have no effect on thermal expansivity as they do not lead to any differential thermal expansion stresses.

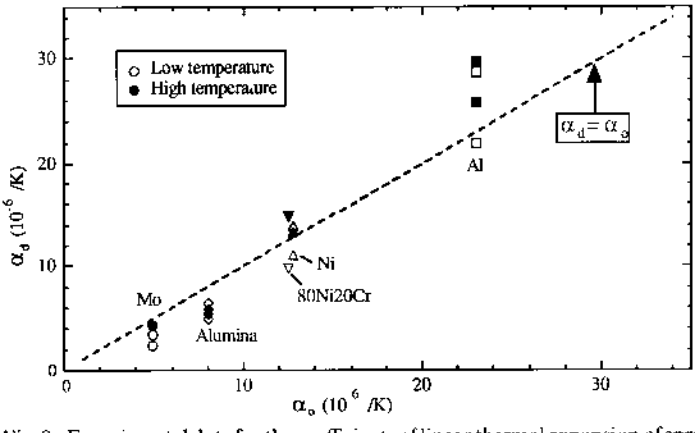

Fig. 8. Experimental data for the coefficients of linear thermal expansion of sprayed materials plotted as a function of the corresponding handbook values.

4.3. Quenching stress data

Measured values of the quenching stress are plotted against the substrate temperature in Fig. 9. Whereas the highest substrate temperature attainable in air was 450 °C, the lowest average temperature during VPS operation was 320 °C. Consequently values from APS cover the lower temperature range whereas those from VPS cover the higher temperature range with an overlapped range of about 100 K. It should be noted that, since the temperature of a substrate in VPS was controlled by intermittent spraying (with a period in between to allow the specimen to cool down to a prescribed temperature), the temperature typically went up from 200 to 600 °C during one cycle of spraying; the average temperature of 400 °C was taken in such a case. The plots above 700 °C were obtained by continuous spraying preceded by preheating, which resulted in a quasi-thermal equilibrium condition and the temperature change during spraying was less than 50 K. Comparing those values between APS and VPS it is rather surprising that they seem to be consistent, despite their very different process environment.

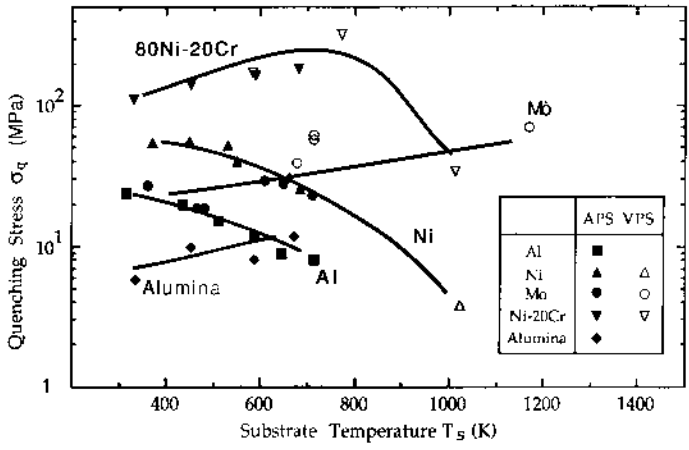

Fig. 9. Dependence of experimental quenching stress values on substrate temperature.

For pure metals, the quenching stresses for the f.c.c. metals nickel and aluminium decrease with temperature, while the value for the refractory b.c.c. metal molybdenum seems to gradually increase with temperature and remains higher than 50 MPa even at 900 °C. The quenching stress in 80Ni–20Cr is markedly higher than that for pure nickel and clearly increases with temperature up to 320 MPa at 500 °C; it then decreases sharply. In contrast, the quenching stress in Al_2O_3 deposits is small, but increases slightly with temperature.

In Fig. 10, the data are replotted onto the substrate temperature normalized by the melting point of each spray material. This figure may be compared with Fig. 11 which shows the applied stress necessary to generate a constant creep strain rate

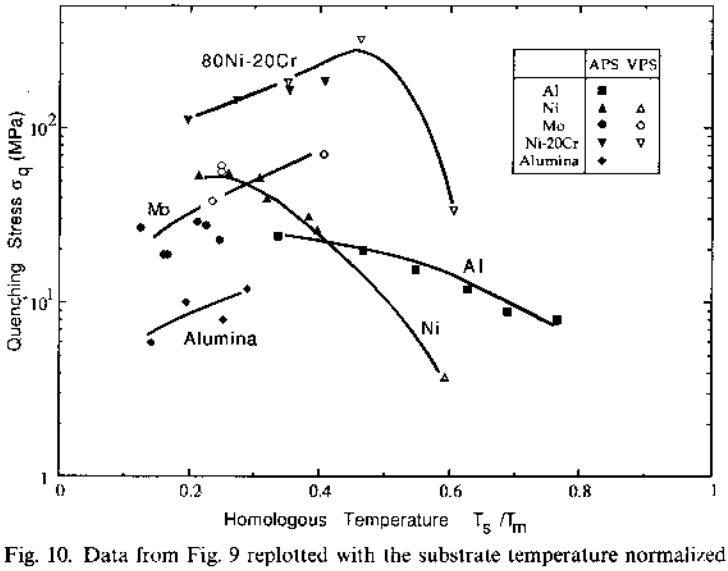

Fig. 10. Data from Fig. 9 replotted with the substrate temperature normalized by the corresponding melting point of spray material.

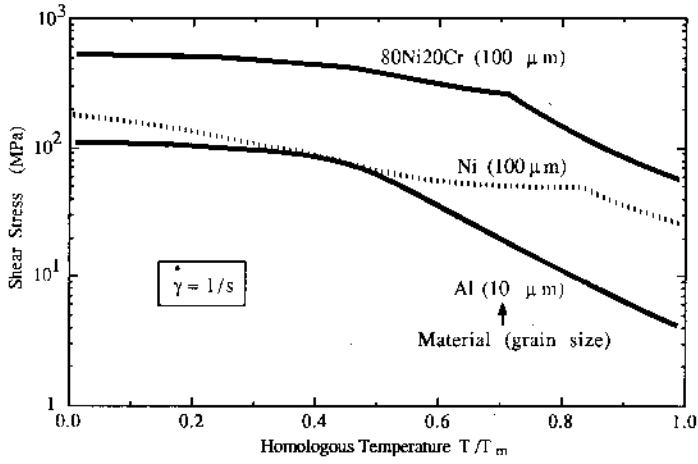

Fig. 11. Handbook data (from Frost and Ashby[27]) showing the applied stress needed to generate a creep rate of $1\ s^{-1}$ as a function of temperature for aluminium, nickel and Ni–20Cr.

$\dot{\gamma} = 1\ s^{-1}$ for three of the metallic materials[27]. (This high strain rate was chosen to see if significant relaxation of stress is possible during the quenching period of a few milliseconds or so.) Values of stresses on the creep curves at $T/T_m = 0.6$ are about 40 MPa (aluminium), 60 MPa (nickel) and 300 MPa (Ni–20Cr) respectively. Since the stress arising from a temperature drop $\Delta T = 100$ K is in the order of 100 MPa (as shown in Table I), it seems that a strain relief in the order of a millistrain could occur by creep as the splat temperature goes down from T_m to $T/T_m = 0.6$. Obviously, if the substrate temperature T_s is high enough, creep continues during the spraying period. Therefore, although such comparisons can only be semi-quantitative at best, it seems likely that creep is largely responsible for the decrease in quenching stress with increasing temperature observed with aluminium and nickel. It may also affect the Ni–Cr for the highest temperature. It is possible that through-thickness yielding (particularly for thick splats) and/or interfacial sliding are also making contributions to the reduction of the quenching stress below its maximum value. The Ni–Cr alloy has a considerably higher yield stress than nickel (and aluminium), as well as a greater creep resistance, so that the higher quenching stress values are entirely as expected.

The observed increase in modulus with substrate temperature seems to indicate that the bonding betweeen splats is stronger at higher temperature, which might explain the increase in quenching stress with temperature exhibited by molybdenum, Ni–Cr and Al_2O_3. For these materials, yielding and creep (which would always tend to increase with temperature) do not appear to be making a significant contribution. At very high substrate temperatures the quenching stress would presumably fall for these materials, indeed this is observed for Ni–Cr at the highest temperature used (as creep would occur and also the modulus would drop), but this regime may well be of no practical significance for many such cases.

For Al_2O_3, the observed quenching stress is more than two orders of magnitude smaller than the yield strength of dense α-Al_2O_3. Even taking account of a possibly lower yield strength of γ-Al_2O_3, it is evident that something is causing a dramatic

reduction in the quenching stress. The obvious explanation is that stress relaxation is taking place by microcracking, as shown in Fig. 12(b), the existence and significance of which have been well documented[8,16]. However, it is unlikely that stress relaxation of such magnitude occurs only by cracking because a considerable proportion of the stress is expected to remain in the fragmented coating if the interface bonding remains sound. Agrawal and Raj evaluated the shear strength of the interface between a silica film and a ductile metal substrate[28]. By stretching the metal plastically, the maximum shear stress at the interface was related to the tensile strength of the film through the distribution of crack spacing in the film. By assuming a sinusoidal distribution of shear stress at the interface, they showed the probable tensile stress distribution within the film after fragmentation, which is still comparable with the tensile strength of the film.

When compared with the work of Agrawal and Raj, the geometry of the present problem is rather different; the radius to thickness ratio of each splat is much smaller than in such thin films. Moreover, plasma-sprayed deposits normally contain a significant amount of small spherical particles (as shown in Fig. 12) which result

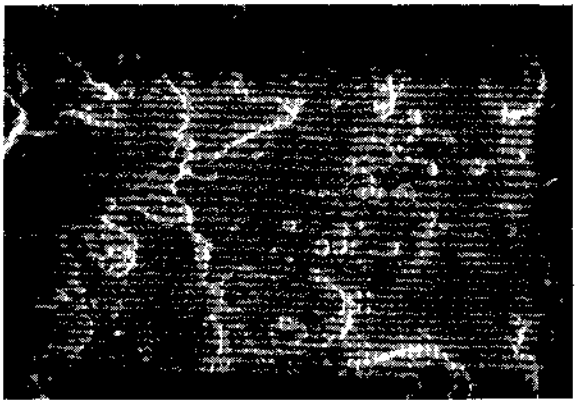

(a)

(b)

Fig. 12. Scanning electron micrograph of the surface of (a) Ni–20Cr and (b) Al_2O_3 alloy sprayed by VPS.

from disintegration of molten droplets in collision and spreading on the solid surface. In such low-aspect ratio splat, stress by quenching must be much smaller because the lateral stress must be zero at free surfaces. (See the edge relaxation mechanism in Fig. 2.) In addition, interfacial sliding probably takes place quite readily with ceramic splats as the microcracking occurs. In general, it is felt that the very low value of the quenching stress in alumina can be understood in the light of such phenomena.

Finally, it should be noted that only two of the stress relaxation mechanisms in Fig. 2, *i.e.* interfacial sliding and microcracking, can also reduce the stiffness for splats assembled into a bulk form. Therefore, as shown in Table IV, the theoretical quenching stress calculated using the actual modulus of deposit $E_d/(T_s)$, rather than the handbook value, is still more than an order greater than the measured σ_q. Evidently, very efficient stress relaxation processes can operate for a splat on a free surface, even when allowance is made for the short time available.

TABLE IV

COMPARISON BETWEEN MEASURED VALUES OF THE QUENCHING STRESS σ_q (FOR T_s = ROOM TEMPERATURE) AND THE THEORETICAL MAXIMUM VALUE σ_0, AND THE CORRECTED VERSION OF THIS, σ_0' CALCULATED USING THE MEASURED MODULUS OF THE DEPOSITS

Material	$\sigma_0 = \alpha_0 \Delta T E_0(T_s)$ (MPa)	$\sigma_0' = \alpha_0 \Delta T E_d(T_s)$ (MPa)	*Measured* σ_q (MPa)
Aluminium	1010	490	25
Nickel	3650	1060	55
Molybdenum	4130	1080	30
Ni–20Cr	3560	1450	110
Al_2O_3	5850	800	10

T_s = room temperature; $\Delta T = T_m - T_s$.

Fig. 13 summarizes the above discussion and shows postulated evolution paths of the stress in a sprayed splat as its temperature T changes from T_m to T_s. For metallic powder (Fig. 13(a)), if it is sprayed onto a substrate at low T_s, stress within a

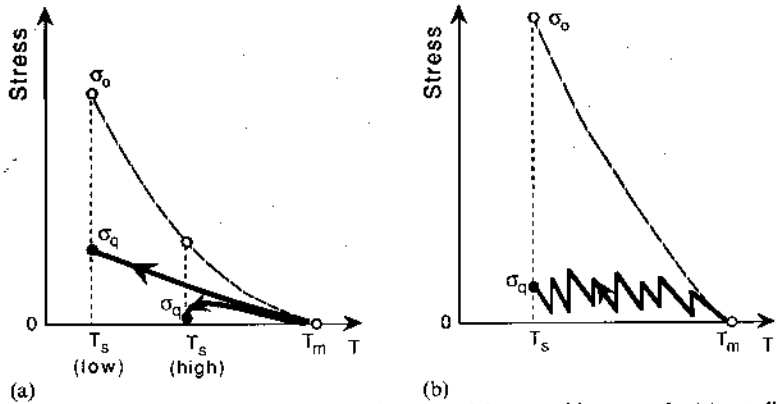

Fig. 13. Schematic depictions of the development of the quenching stress for (a) metallic and (b) ceramic deposits.

splat would increase monotonically as the maximum stress shown by the broken curve is reduced by the various relaxation mechanisms. If T_s is high, the splat would undergo more stress relaxation, particularly creep, because the time spent in the high temperature regime must be longer than the low T_s case and the splat could even experience isothermal creep at T_s. For ceramic powder (Fig. 13(b)), the local stress would follow a saw-like path, as repeated microcracking in the vicinity relieves the stress instantaneously. Averaged over the specimen, the effect would be to maintain σ_q at a very low level throughout cooling.

5. CONCLUSIONS

Thermal and mechanical properties of plasma-sprayed materials such as Young's modulus, coefficient of linear thermal expansion and quenching stress have been studied. Table V summarizes the experimental results in comparison with dense bulk materials.

TABLE V

SUMMARY OF EXPERIMENTAL RESULTS. YOUNG'S MODULUS E_d AND COEFFICIENT OF THERMAL EXPANSION α_d OF PLASMA SPRAYED MATERIALS ARE COMPARED WITH VALUES OF DENSE BULK MATERIALS E_0 AND α_0. FOR QUENCHING STRESS σ_q LOWER BOUND AND UPPER BOUND VALUES ARE GIVEN WITH TEMPERATURE DEPENDENCE IN PARENTHESIS

Material	E_d	α_d	σ_q
Aluminium, nickel	$E_0/3$	$\approx \alpha_0$	$4 \approx 60$MPa(−)
Molybdenum	$E_0/3$	$\approx \alpha_0$	$20 \approx 60$MPa (+)
80Ni–20Cr	$E_0/3$	$\approx \alpha_0$	$35 \approx 320$MPa (+/−)
Al_2O_3	$E_0/6$	$\approx \alpha_0$	≈ 10MPa (+)
Temperature range	Room temperature	Room temperature ~ 300 °C	50 ~ 900 °C

1. The Young's modulus of metallic deposits is about one third that of dense materials, whereas that of Al_2O_3 is significantly lower than this.

2. No significant differences have been observed in thermal expansivity from those for the dense materials, in agreement with theoretical expectation.

3. The soft f.c.c. metals aluminium and nickel have quenching stresses of 20–50 MPa when deposited on substrates below 100 °C; these values decrease with increasing substrate temperature. Molybdenum shows a similar range of values, but in this case the value increases with increasing substrate temperature—at least up to an homologous temperature of about 0.5 T_m. The Ni–Cr alloy exhibits the highest quenching stress among the materials tested; it is well over 100 MPa, with a positive temperature dependence up to a maximum value of 320 MPa at 500 °C, after which it drops sharply by about an order of magnitude at temperature of around 700 °C. Alumina exhibits the lowest quenching stress values, at around 10 MPa, with fairly weak temperature dependence.

Finally, the significance of these properties has been discussed in terms of residual stress. For Al_2O_3, and probably for other brittle ceramics too, the thermal

stresses would dominate in most cases, because the quenching stress is very small and there is often a large difference in thermal expansivity between a ceramic coating and a metallic substrate. (However, in heat flow calculations and in evaluation of the thermal stress, it is essential to treat elastic moduli and thermal conductivity properly, as these can differ markedly from those of the corresponding dense materials[29,30]. Furthermore, the values cannot reliably be predicted by a simple rule-of-mixtures from a knowledge of the porosity level.) For metallic materials, on the other hand, the quenching stress can be very significant, especially for alloys with a high creep resistance and yield strength. Other material properties are in general not so drastically different from those of the corresponding dense materials.

Numerical modelling which incorporates realistic quenching stresses and appropriate *in situ* material properties should prove to be a versatile tool in controlling and assessing the stress state of various sprayed materials, including cases of high complexity such as multi-layered coatings, composite coatings and functionally graded materials.

ACKNOWLEDGMENTS

We would like to thank Mr. H. Takagi for carrying out many of the experiments using APS and Mr. K. A. Roberts for his expertise in carrying out experiments using VPS. We are also grateful to Dr. K. Kishii of Toshiba Glass Co. for the thermal expansivity measurement. We have also had valuable discussions with Mr. S. C. Gill of Cambridge University. Thanks are extended to Science and Engineering Research Council/Ministry of Defence for supporting the VPS facility and to Showa Denko K.K. for supplying some of the spray powders.

REFERENCES

1 R. C. Hendricks, G. McDonald and R. L. Mullen, *Ceram. Eng. Sci. Proc., 4* (1983) 802.
2 S. Kitahara, K. Hyakutake and M. Ishida, *Proc. 11th Int. Thermal Spraying Conf., Montreal, 1986*, Pergamon, New York, 1986, p. 785.
3 J. W. Watson and S. R. Levine, *Thin Solid Films, 119* (1984) 185.
4 R. Kingswell, K. T. Scott and D. T. Gawne, *Proc. 1st Int. Conf. on Plasma Surf. Eng. Garmisch Parterkirchen*, DGM, 1989, p. 695.
5 W. E. Ballard, *Metal Spraying and the Flame Deposition of Ceramics and Plastics*, Griffin, London, 4th end., 1963, p. 785.
6 S. J. Harris, R. C. Cobb and H. James, *Proc. 10th Int. Thermal Spraying Conf., Essen, 1983*, Deutscher Verlag für Schweißtechnik GmbH, Düsseldorf, 1983, p. 245.
7 J. H. Zaat, *Ann. Rev. Mater. Sci., 13* (1983) 9.
8 R. McPherson, *Thin Solid Films, 83* (1981) 297.
9 W. E. Ballard, *Metal Spraying and the Flame Deposition of Ceramics and Plastics*, Griffin, London, 4th edn., 1963, pp. 387–393.
10 S. Kuroda, T. Fukushima and S. Kitahara, *Vacuum, 41* (1990) 1297.
11 C. W. Marynowski, F. A. Halden and E. P. Farley, *Electrochem. Technol., 3* (1965) 109.
12 D. Lee, *Int. J. Mech. Sci., 25* (1983) 543.
13 D. S. Rickerby, K. T. Scott, G. Eckold and D. Lloyd-Thomas, *Proc. 1st Plasma-Technik-Symp.*, Vol. 2, Lucerne, 1988.
14 S. C. Gill and T. W. Clyne, *Metall. Trans. B, 21* (1990) 377.
15 S. C. Gill and T. W. Clyne, *Property data evaluation for the modelling of residual stress development*

during vacuum plasma spray deposition. In H. E. Exner, and V. Schumacher (eds.), *Advanced Materials and Processes—Euromat 89*, DGM, 1990, pp. 1221–1230.
16 S. C. Gill and T. W. Clyne, in P. Vincinzini (ed.), *Proc. 7th Cimtec World Ceramic Cong.*, 1990, paper No.S1.2A–L07.
17 S. Kuroda, T. Fukushima and S. Kitahara, *Thin Solid Films*, *164* (1988) 157.
18 S. P. Timoshenko and J. M. Gere, *Mechanics of Materials*, D. Van Nostrand, New York, 1972, p. 142.
19 T. A. Hahn, *J. Appl. Phys.*, *41* (1970) 5096.
20 G. Stoney, *Proc. Roy. Soc. London, A82* (1909) 172.
21 A. Brenner and S. Senderoff, *J. Res. Natl. Bur. Stand.*, *42* (1949) 105.
22 J. D. Eshelby, *Proc, Roy. Soc.*, *A252* (1959) 561.
23 R. McPherson and B. B. Shafer, *Thin Solid Films*, *97* (1982) 201.
24 D. Fargeot, F. Platon and P. Buch, *Sci. Ceram.*, *9* (1977) 382.
25 A. Noutomi, M. Kodama, T. Ono, Y. Inoue, M. Kawano and N. Tani, *Yousetsu Gakkai Ronbunshu*, *6* (1988) 341 (in Japanese).
26 B. D. Cullity, *Elements of X-ray Diffraction*, Addison-Wesley, Massachusetts, 2nd edn., 1987, p. 472.
27 H. J. Frost and M. F. Ashby, *Deformation- Mechanism Maps*, Pergamon, Oxford, 1982.
28 D. C. Agrawal and R. Raj, *Acta Metall.*, *37* (1989) 1265.
29 R. McPherson, *Thin Solid Films*, *112* (1984) 89.
30 T. W. Clyne and S. Kuroda, submitted to *Acta Metall.*

APPENDIX A: NOMENCLATURE

α_d	coefficient of thermal expansion of deposit
α_s	coefficient of thermal expansion of substrate
β	ratio of Young's modulus of deposit to that of substrate
E_d	Young's modulus of deposit
E_0	Young's modulus of dense material
E_s	Young's modulus of substrate
$\dot{\gamma}$	strain rate
h_d	thickness of deposit
h_s	thickness of substrate
ν	Poisson's ratio
$1/R$	curvature of substrate
ρ	density
T	temperature of sprayed splat
T_m	melting point of spray material
T_0	ambient temperature
T_s	substrate temperature during spraying
T_s	substrate temperature during spraying which results in zero residual stress